5.5 A Stacking Mixer-First Receiver Achieving >20dBm Adjacent-Channel IIP3 Consuming less than 25mW

Stef van Zanten, Ronan van der Zee, Bram Nauta

University of Twente, Enschede, The Netherlands

The sub-6GHz spectrum is used by many standards including 5G New Radio. In this crowded spectrum, an RX requires good linearity and flexibility to address different bands without separate SAW filters, whilst maintaining low NF. Traditional mixer-first receivers (MF-RX) offer this flexibility while postponing voltage amplification to the end of the RX chain, benefiting linearity but leading to relatively poor NF. LNTA-based designs [1,2] offer an alternative: initial amplification alleviates noise constraints, but the pole at the LNTA output limits the RX operating range, though efforts to reduce parasitic capacitance have been fruitful [2]. Still, linearity is impacted by this initial voltage gain, which is typically addressed by deploying an N-path notch filter in feedback around the LNTA, but its slope is generally limited to 20dB/decade, reflecting in poor adjacent channel IIP3. Although solutions to increase this slope exist, the extra circuitry increases the RF parasitics and power consumption. Also, in contrast to an MF-RX which has a low-ohmic OOB path to ground, the LNTA output stage has to fully absorb any out-of-band (OOB) interferer currents.

Recently, MF-RX have become more viable as passive voltage gain through capacitor stacking has improved NF and aided integration of harmonic rejection. However, the larger swing aggravates V_{GS} switch modulation, reflecting in a moderate in-band (IB) IIP_3, emphasizing the need for steep filtering already at the MF-RX BB capacitor. To improve selectivity, complex BB impedances consisting out of inductors and gyrators can be synthesized, but at the cost of higher power and complexity [3]. A simpler alternative designs the MF-RX with an enlarged BB capacitor in combination with a negative capacitance (synthesized through positive feedback) that restores the IB signal to the desired BW. By rolling-off this negative capacitance OOB, the MF-RX selectivity can be doubled to 40dB/decade [4,5], but the extend of this steeper roll-off is directly coupled to NF deterioration.

In this work, we break the direct trade-off between NF and selectivity improvement due to positive capacitive feedback. We recognize that capacitive feedback can be used to not only decrease the apparent baseband capacitance C_B through positive feedback, but also increase it by using negative feedback, see Fig. 5.5.1. Here, we combine the best of both worlds: by using positive feedback IB and negative feedback OOB we greatly improve the receiver's interferer rejection without taking a severe NF penalty. The starting point is a baseband capacitor C_B that is larger than required for the specified BW (f_c). Using positive feedback, we decrease the effective capacitance C_{eff} (and thus increase the apparent MF-RX baseband impedance Z_{BB}) to the needed value in-band, see (1) in Fig. 5.5.1. Moving to OOB frequencies, we transition the positive feedback into negative feedback, resulting in a 60dB/decade slope, much larger than for traditional positive capacitive feedback only. In addition, negative feedback allows us to make the effective OOB capacitance significantly larger than C_B alone over a wide frequency range, thus lowering Z_{BB} and improving interferer rejection (see (2) in Fig. 5.5.1), boosting adjacent channel and far-OOB IIP_3. For frequencies higher than the loop BW ($f_{c\text{-}loop}$), the larger C_B that we started with keeps the OOB impedance low. Furthermore, to enable a low NF, we combine the capacitive feedback with a stacking MF-RX design offering 2× passive voltage gain (see (3) in Fig. 5.5.1), which we optimized for a wide LO operating range by making C_B larger than C_R similar to [6], reducing parasitics at the RF node.

Figure 5.5.2 (top-right) shows the block diagram. Compared to a stacking MF-RX without capacitive loop, we make C_B 2× larger (C_B = 2C) than required for the desired BW, while we use a feedback capacitor C_M = C. To realize the Z_{BB} illustrated in Fig. 5.5.1, A(f) implements both a 2nd-order magnitude increase and a phase inversion around the band edge (f_c). The first block of A(f) provides voltage gain (-10×) for the RX chain and a subsequent output, relaxing the noise requirements of the rest of the feedback network. The required phase transition and magnitude increase are implemented using a dual-path approach, consisting of: 1) an IB path that provides frequency independent attenuation; and 2) an OOB path that increases the feedback's magnitude beyond the band edge. Due to the initial -10x voltage gain in the feedback network, the OOB path can be implemented with a simple 2nd-order HPF. A summation of both paths yields the desired shelf-like response of A(f) (Fig. 5.5.2 – left), realizing a left- (LHP) and a right-half-plane (RHP) zero at the transition point from the IB to the OOB path. The two poles at the cut-off frequency of the HPF rotate the phase 180 degrees, resulting in strong negative feedback. The 40dB/decade magnitude increase and phase rotation in the HPF yield a closed-loop selectivity of almost 60dB/decade, benefiting linearity. We guarantee stability by limiting the IB positive loop gain, including the 1/3 C_M to C_B voltage division, to below 0dB and by providing > 60 degree phase margin at both 0dB crossings. Figure 5.5.2 (bottom-right) illustrates this using a Nyquist plot of the complete loop gain T(jω). The S_{11} stays below 0dB across the spectrum, guaranteeing stability for varying source impedances.

Figure 5.5.3 shows the circuit diagram of the MF-RX. A stacking front-end provides 2× passive voltage gain, benefiting NF. Resistor R_{match} provides input matching and has been placed in feedback around the initial voltage gain block (-10×) in A(f) to limit its noise contribution. This first voltage amplifier consists of a gm and TIA combination, in which the TIA virtual ground minimizes V_{DS} non-linearity in the CMOS inverter that implements the gm. The HPF in the OOB path uses a Sallen-Key topology; the designed complex poles fasten the A(f) phase transition, benefitting MF-RX filter steepness. The specs of the HPF's internal 5T opamp are relaxed due to both the gain up-front and the buffering feedback OTA. In our design, this OTA serves three purposes: 1) it sums the IB and OOB path; 2) it provides the attenuation for the IB path using a PVT-robust capacitor ratio; and 3) it buffers the feedback signal so that C_M can be driven up to frequencies far OOB. We use the same inverter-based design that maximizes open-loop gain and BW for both OTAs in the feedback loop, but these could be separately optimized if required.

The MF-RX has been implemented in 22nm FDSOI (Fig. 5.5.7). Figure 5.5.4 shows transfer function and NF measurements. The BW is boosted from 10MHz to 20MHz due to positive feedback, while a selectivity of 14dB/octave (well over 40dB/decade) is achieved because of negative feedback OOB. The loop BW is approximately 200MHz, achieving over a decade of increased-rejection frequency range. S_{11} is < -4dB across the LO operating frequency (1.2 to 6.0GHz), while the RF losses are limited to 0.7dB at 6 GHz with respect to the maximum 32dB RF-to-BB gain. At 3GHz, an optimum NF of 4.8dB is achieved which increases to 5.2dB at 1.2GHz due to the MF-RX going into the sampling region and to 5.5dB at 6GHz due to RF losses. A blocker NF of 16.7dB has been measured at a 1.4GHz LO with a 0dBm blocker at $6f_c$ offset. Figure 5.5.5 shows linearity measurements. Due to the increased selectivity, adjacent channel IIP_3 ($\Delta f = 2f_c$) is boosted from 7dBm (loop off) to 22dBm (loop on), with linearity improvements persisting to almost two decades OOB. Notches in IIP_3 of <5dB can be observed corresponding to the small OOB magnitude increase in S_{21} in Fig. 5.5.4. The adjacent channel IIP_3 varies less than 5dB over the LO operating range. A maximum IIP_2, IIP_3 and B_{1dB} of 79, 28 and 0.5dBm respectively are achieved.

Figure 5.5.6 compares the designed MF-RX to state-of-the-art LNTA-based and MF-RX designs [1-5]. The implemented loop realizes steep filtering, benefiting linearity, which reflects in an excellent adjacent channel IIP_3 of >20dBm, outperforming the LNTA-based designs by more than 10dB [1,2]. Although the MF-RX designs [3] and [5] have similar adjacent channel IIP_3, they have a much lower gain, while they use over 7× more power at a 4GHz f_{LO}. Overall, this work consumes the lowest power, varying from 12.7mW at 1.2GHz to 24.7mW at 6GHz, while achieving >20dBm adjacent channel IIP_3 across the full LO operating range.

Acknowledgement:
The authors would like to thank GlobalFoundries for providing silicon fabrication through the 22FDX university program. This project has received funding from the European Research Council (ERC) under the European Union's Horizon 2020 research and innovation programme (grant agreement No 834389).

References:
[1] H. Razavi and B. Razavi, "A 0.4–6 GHz Receiver for Cellular and WiFi Applications," *IEEE JSSC*, vol. 57, no. 9, pp. 2640-2657, Sept. 2022.
[2] M. A. Montazerolghaem et al., "19.1 A 300MHz-BW, 27-to-38dBm In-Band OIP3 sub-7GHz Receiver for 5G Local Area Base Station Applications," *ISSCC*, pp. 292-293, Feb. 2023.
[3] S. Krishnamurthy and A. M. Niknejad, "An Enhanced Mixer-First Receiver With Distortion Cancellation, Achieving 80-dB/decade RF Selectivity and +8-dBm B1dB for Adjacent Channel Blockers," *IEEE SCC-L*, vol. 4, pp. 64-67, 2021.
[4] G. Pini et al., "Analysis and Design of a 260-MHz RF Bandwidth +22-dBm OOB-IIP3 Mixer-First Receiver With Third-Order Current-Mode Filtering TIA," *IEEE JSSC*, vol. 55, no. 7, pp. 1819-1829, July 2020.
[5] Y. -C. Lien et al., "Enhanced-Selectivity High-Linearity Low-Noise Mixer-First Receiver With Complex Pole Pair Due to Capacitive Positive Feedback," *IEEE JSSC*, vol. 53, no. 5, pp. 1348-1360, May 2018.
[6] S. Weinreich and B. Murmann, "A 0.6–1.8-mW 3.4-dB NF Mixer-First Receiver With an N-Path Harmonic-Rejection Transformer-Mixer," *IEEE JSSC*, vol. 58, no. 6, pp. 1508-1518, June 2023.

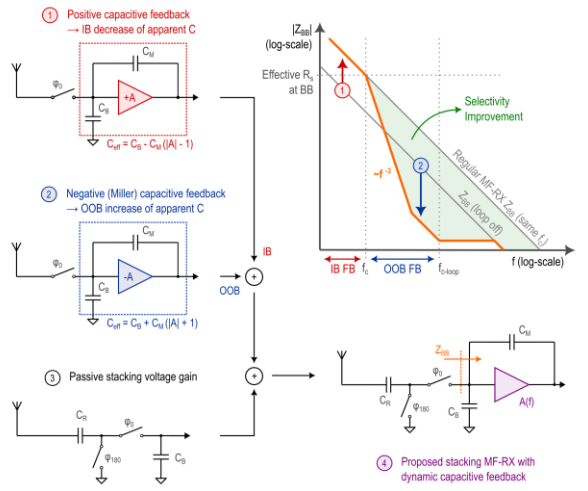

Figure 5.5.1: Key concept of the stacking MF-RX with selectivity-enhancing feedback loop based on capacitive feedback.

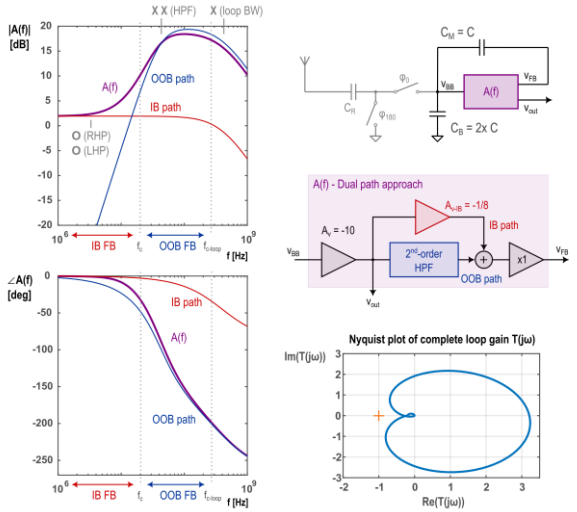

Figure 5.5.2: Block-level design of the dual-path feedback loop in the MF-RX, including verification of loop stability in a Nyquist plot.

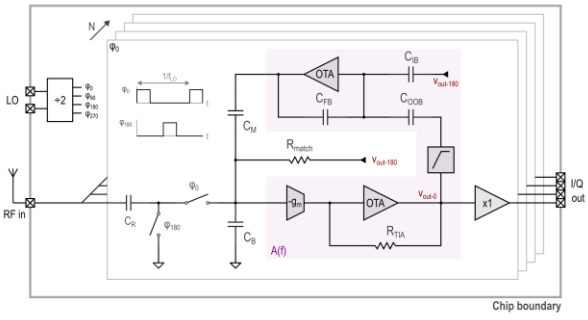

Figure 5.5.3: Block-diagram of the MF-RX with capacitive feedback loop (biasing not shown).

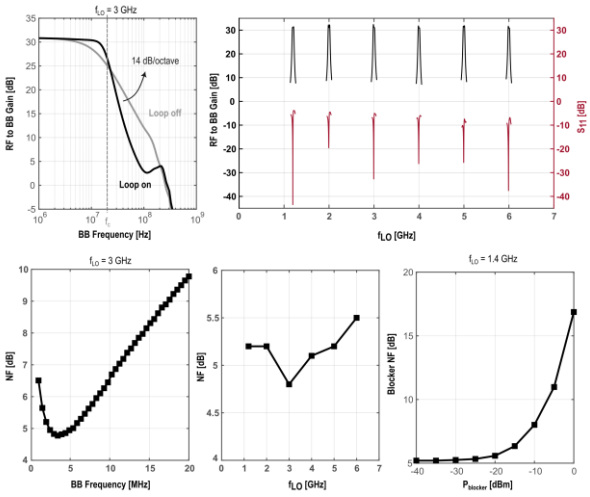

Figure 5.5.4: Measured RF to BB gain, S11, NF over a baseband and LO sweep and blocker NF.

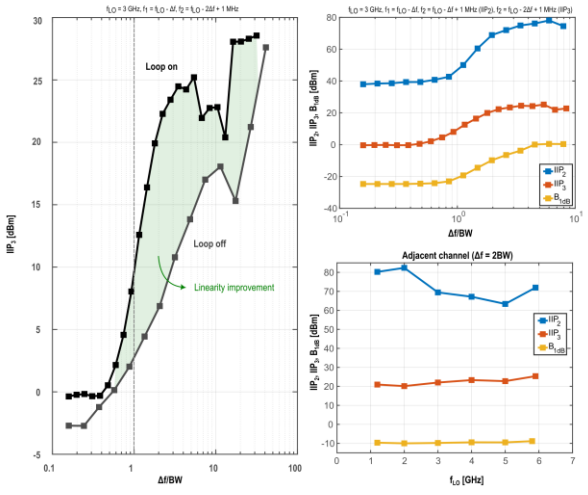

Figure 5.5.5: Linearity measurements of the MF-RX.

	This Work	Montazerolghaem ISSCC 2023 [2]	Razavi JSSC 2022 [1]	Krishnamurthy SSC-L 2021 [3]	Pini JSSC 2020 [4]	Lien JSSC 2018 [5]
Architecture	MF-RX	LNTA based	LNTA based	MF-RX	MF-RX	MF-RX
CMOS Technology	22 nm SOI	40 nm	28 nm	28 nm	28 nm	45 nm SOI
RF Input	Single-ended	Single-ended	Single-ended	Single-ended	Differential	Differential
Frequency Range [GHz]	1.2 – 6	0.4 – 7.3	0.4 - 6	0.2 – 3.5	0.5 – 2	0.2 – 8
Gain [dB]	32	38	54	16	32	21
BB BW [MHz]	20	150	0.1 – 80	15	130	10
NF [dB]	4.7 – 5.5	3.2 – 5.8	3.2[1,3]	6.6 – 12	5.5[9]	2.3 – 5.4[11]
NF Degradation @ fc [dB]	+5	+2.8[1]	+0.2[1,3]	N/A	+6.8[1,10]	+0.2[1,10]
0 dBm OOB BNF [dB]	16.7	9.7	5.2[4]/7.4[5]	9	N/A	4.7
Adjacent channel IIP3 [dBm] (@ 2fc)	20 – 25	10[1]	-26[1,6]	23	12[1]	16[1]
Max. OOB IIP3 [dBm] (@ Δf/fc)	28 (40)	11 (3)	3 (50)[6]	24 (10)[7]	21 (3)	39 (8)
IB IIP3 [dBm]	-1	-11 – 0[2]	-35[1,2,8]	3[1]	-12[1]	0[1]
OOB IIP2 [dBm] (@ Δf/fc)	79 (6)	68 (3)	28 (50)[1,6]	N/A	70 (3)	88 (8)
OOB B1dB [dBm] (@ Δf/fc)	0.5 (5)	-4.8 (3)	N/A	11 (10)[1]	3 (6)	12 (8)
Supply [V]	0.8	1.3	1	1.2/1.4	1.8/1.2	1.2
Active area [mm²]	0.22	0.42	1.9[7]	1.5[7]	0.16	0.8
Power [mW]	9.7 + 2.5 mW/GHz	100 + 13 mW/GHz	23 – 49 13 – 39[8]	89 – 149	21.6 + 7.8 mW/GHz	50 + 30 mW/GHz

[1] Estimated from plots. [2] IB OIP3 minus gain. [3] NF for 40 MHz channel-bandwidth case, at 5 GHz LO. [4] Low-noise mode. [5] Harmonic rejection mode. [6] 40 MHz channel-bandwidth case. [7] Complete die area. [8] Excluding harmonic traps. [9] NF at 2 GHz LO. [10] Simulation data. [11] NF reported for 0.5 – 6 GHz LO.

Figure 5.5.6: Comparison with state-of-the-art LNTA-based and MF-RX designs.

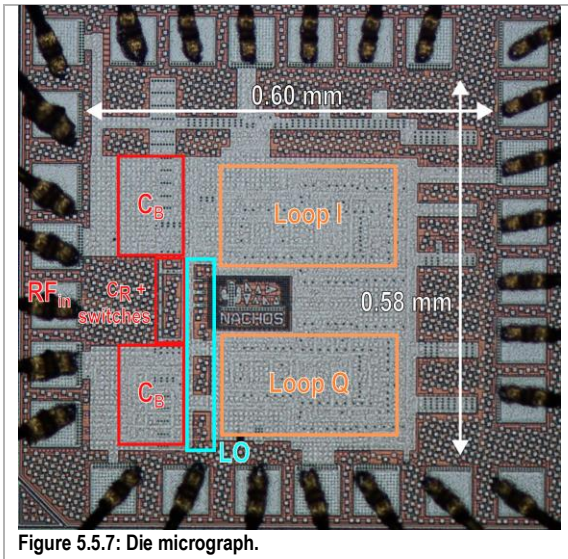

Figure 5.5.7: Die micrograph.